

GEOCHEMISTRY

A nanocrystalline monoclinic CaCO_3 precursor of metastable aragonitePéter Németh^{1*†}, Enrico Mugnaioli^{2*}, Mauro Gemmi², György Czuppon³, Attila Demény³, Christoph Spötl⁴

Despite its thermodynamical metastability at near-surface conditions, aragonite is widespread in marine and terrestrial sediments. It abundantly forms in living organisms, and its abiotic formation is favored in waters of a $\text{Mg}^{2+}/\text{Ca}^{2+}$ ratio > 1.5 . Here, we provide crystallographic evidence of a nanocrystalline CaCO_3 polymorph, which precipitates before aragonite in a cave. The new phase, which we term monoclinic aragonite (mAra), is crystallographically related to ordinary, orthorhombic aragonite. Electron diffraction tomography combined with structure determination demonstrates that mAra has a layered aragonite structure, in which some carbonates can be replaced by hydroxyls and up to 10 atomic % of Mg can be incorporated. The diagnostic electron diffraction features of mAra are diffuse scattering and satellite reflections along aragonite {110}. Similar features have previously been reported—although unrecognized—from biogenic aragonite formed in stromatolites, mollusks, and cyanobacteria as well as from synthetic material. We propose that mAra is a widespread crystalline CaCO_3 that plays a hitherto unrecognized key role in metastable aragonite formation.

INTRODUCTION

Calcium carbonate is known to occur naturally as three anhydrous crystalline structures (polymorphs): aragonite, calcite, and vaterite. Aragonite is the high-pressure polymorph, whereas calcite is the thermodynamically stable phase at ambient conditions. The stability field of vaterite is not well established, but its occurrence is commonly associated with the first stages of CaCO_3 precipitation and nanosized crystal formation (1–3). Calcite and aragonite are, by far, the most abundant naturally occurring calcium carbonates. Although aragonite is metastable at Earth's near-surface conditions, it is widespread in marine and also in terrestrial environments (4, 5).

The formation of metastable aragonite is attributed to abiotic and biotic factors. Abiotic precipitation is favored in waters with a $\text{Mg}^{2+}/\text{Ca}^{2+}$ ratio > 1.5 ($\text{pH} > 8.2$) (6) and a saturation index of calcite < 0.8 (7). Ab initio thermodynamic calculations explain metastable aragonite precipitation by the increasing surface energy of calcite upon Mg uptake. The surface energy of aragonite decreases compared to Mg calcite at $\text{Mg}^{2+}/\text{Ca}^{2+} > 2.0$, thus favoring aragonite formation (8). Biogenic aragonite abundantly forms in mollusk shells (9–11), warm- and cold-water corals (12), serpuloid worms (13), fish otoliths (14), and stromatolites (15). Protein macromolecules produced by these organisms modify the physicochemical microenvironment, thus providing favorable conditions for aragonite relative to calcite formation (11, 16, 17).

Amorphous calcium carbonate (ACC) is commonly reported as a precursor phase of crystalline, and in particular biogenic, CaCO_3 (18). Aragonite precursor ACC, referred to as protoaragonite (pAra), has been reported from corals (19) and mollusk shells (20). Similarly,

hydrous ACC has also been observed as a precursor of crystalline CaCO_3 in laboratory experiments (21–23). This phase transforms into aragonite via anhydrous ACC (8) or via monohydrocalcite (24). During these steps, a series of ordering, dehydration, and crystallization processes occur, which lower the free energy of the system (25). Although these amorphous precursors provide insights into the

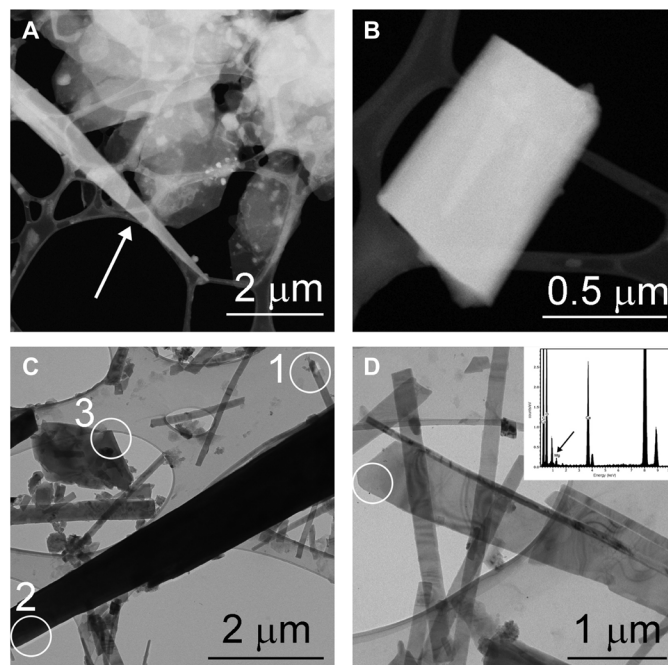


Fig. 1. mAra from the drip water sample and from the top layer of the aragonite flowstone. (A) Flaky hydromagnesite particles occur together with an elongated mAra crystal (white arrow) in the drip water sample. (B) Tabular mAra grain from the same sample. (C) Aragonite (1) is associated with needle-shaped (2) and flaky (3) mAra crystals in the flowstone sample. The SAED patterns of these crystals are shown in Fig. 2. (D) Mg-bearing elongated mAra crystal from the flowstone sample. Chemical analyses obtained from the white circle area indicate ~ 10 atomic % Mg (black arrow).

¹Institute of Materials and Environmental Chemistry, Research Centre for Natural Sciences, Hungarian Academy of Sciences, Magyar tudósok körútja 2, Budapest 1117, Hungary. ²Center for Nanotechnology Innovation@NEST, Istituto Italiano di Tecnologia (IIT), Piazza San Silvestro 12, Pisa 56127, Italy. ³Institute for Geological and Geochemical Research, RCAES, Hungarian Academy of Sciences, Budaörsi út 45, Budapest 1112, Hungary. ⁴Institute of Geology, University of Innsbruck, Innrain 52, Innsbruck 6020, Austria.

*These authors contributed equally to this work.

†Corresponding author. Email: nemeth.peter@ttk.mta.hu

formation of some synthetic and biogenic aragonite, the abundant formation of metastable aragonite in natural environments is still poorly understood.

Here, we investigate the first carbonate precipitates (Fig. 1) occurring in a cold cave decorated by aragonite speleothems (26) and provide evidence of a new nanocrystalline calcium carbonate polymorph—which we term monoclinic aragonite (mAra)—that forms from Mg-rich ($\text{Mg}^{2+}/\text{Ca}^{2+} > 1.5$) drip water. This phase appears to precipitate before the conventional, orthorhombic aragonite and plays a key role in metastable aragonite formation. mAra is crystallographically related to aragonite, associated with hydromagnesite [$\text{Mg}_5(\text{CO}_3)_4(\text{OH})_2 \cdot 4\text{H}_2\text{O}$] and magnesite (MgCO_3), and with time transforms to aragonite. We use transmission electron microscopy (TEM) and selected-area electron diffraction (SAED) to characterize this nanocrystalline phase and apply the state-of-the-art electron diffraction tomography (EDT) technique (27–29) to determine its crystal structure (see Materials and Methods). We propose a mechanism explaining metastable aragonite formation in Mg-rich environments ($\text{Mg}^{2+}/\text{Ca}^{2+} > 1.5$), that is, at conditions where aragonite abundantly precipitates.

RESULTS

Fresh carbonate precipitates

Both Mg- and Ca-containing carbonates occur in the precipitates sampled from the stalactite drip water and from the outermost layer

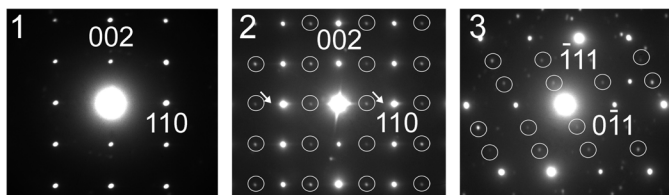


Fig. 2. Compared to aragonite (1), the characteristic diffraction features of mAra (2 and 3) are the occurrence of satellite reflections. Satellites are marked by white circles. White arrows of (2) show streaking of reflections along $\{110\}$ indicating disorder. Sample thickness gives rise to $\{001\}$ reflections. The corresponding crystals of these SAED patterns are shown in Fig. 1C.

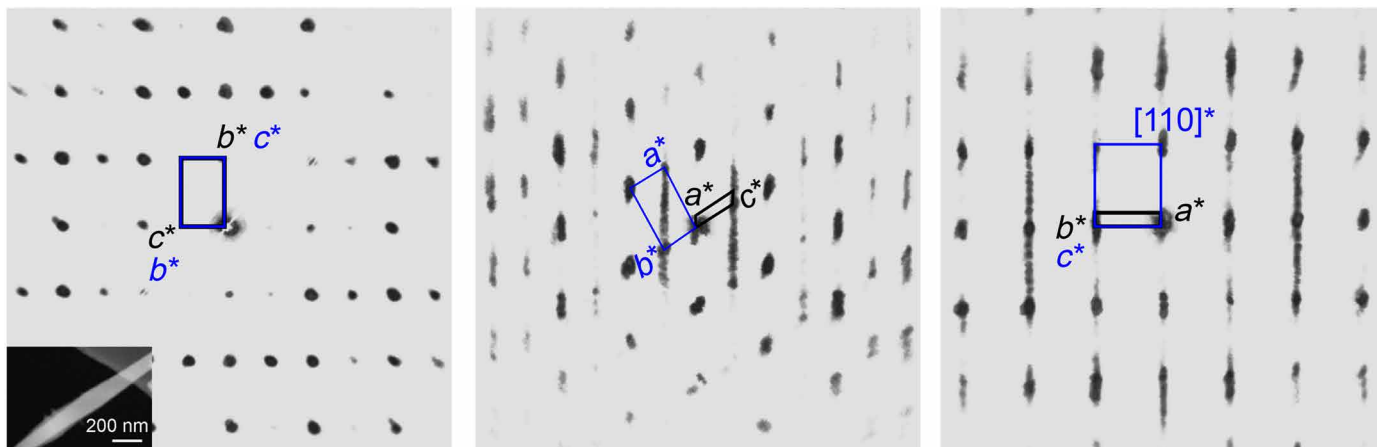


Fig. 3. Principal two-dimensional slices of the reciprocal lattice highlight diffuse scattering and satellite reflections of aragonite and reveal the crystallographic relationship between aragonite and mAra. The slices are reconstructed from the three-dimensional EDT volume. The measured grain is shown in the lower left corner of the first panel. Black and blue lines mark mArA and aragonite unit cells, respectively. mAra and aragonite crystallographic axes are labeled by black and blue indices, respectively. Diffuse scattering runs along the $\{110\}$ diagonal of aragonite cell, breaks its orthorhombic symmetry, and indicates modulation. Discrete satellite reflections suggest that the unit cell of mAra is monoclinic, and the unit-cell parameter a is $28.6(7)$ Å.

of aragonite flowstone (fig. S1), but their proportions differ. The first carbonate precipitates, collected from the drip water, are dominated by Mg carbonates, whereas the surface of flowstone contains abundant Ca-carbonates.

The drip water sample yields submicrometer- to several micrometer-size pseudo-hexagonal Mg-carbonate platelets (Fig. 1A and fig. S2). EDT measurements show that they are hydromagnesite, and the data permit the ab initio determination of all Mg, C, and O atoms (Materials and Methods and table S3). Closely associated with hydromagnesite, Ca-carbonate crystals are found both as triangular needles and as rectangular grains (Fig. 1, A and B). EDT measurements of these particles show diffraction volumes consistent with the orthorhombic aragonite cell, which, however, are characterized by strong diffuse scattering along $\{110\}$.

The surface of the wet aragonite flowstone contains Mg carbonates in the form of nanosize magnesite flakes (fig. S3) and abundant Ca-carbonates that resemble the Ca-carbonate particles precipitated from drip water based on their shape and diffraction features (Fig. 1, C and D). Acicular crystals (20 to 50 nm wide and 1 to 2 μm long) occur together with larger rhombic grains and 200- to 400-nm-wide and several-micrometer-long triangular needles. While some grains correspond to aragonite, the majority of grains show diffraction features inconsistent with the aragonite structure. In particular, SAED patterns reveal satellite reflections that occur next to ordinary aragonite reflections, and imply that the symmetry and structure of these crystals differ from those of ordinary, orthorhombic aragonite (Fig. 2). Because these diffraction patterns suggest a monoclinic unit cell, we refer to this crystal type as mAra.

Crystal structure of mAra

EDT measurements of several grains show that the diffraction pattern of mAra differs from that of aragonite by the occurrence of diffuse scattering and satellite reflections along aragonite $\{110\}$ (Fig. 3). The measured crystals show notable variability in the intensity ratio between satellite reflections and diffuse scattering, which implies a different degree of ordering in the crystal stacking along aragonite $\{110\}$. The higher the diffuse scattering contribution, the less ordered the stacking sequence. Even the best EDT dataset (Fig. 3 and

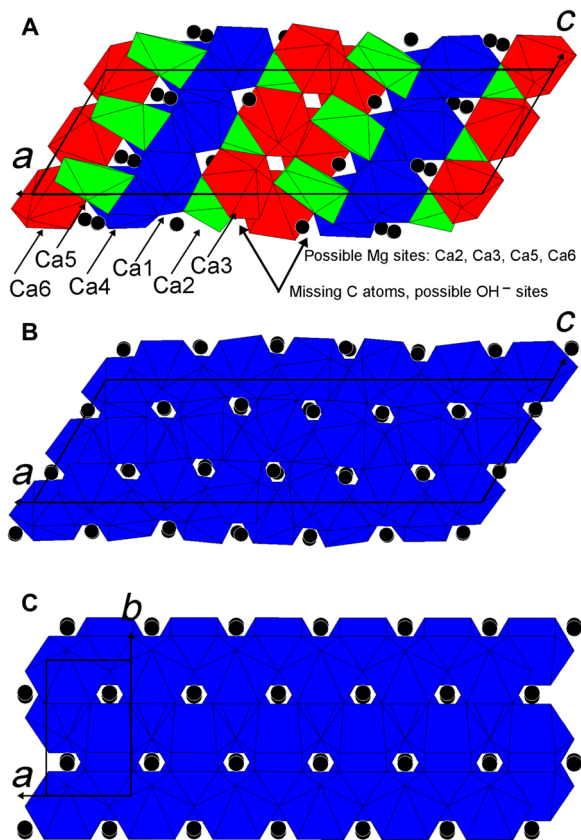


Fig. 4. Structure models of mAra in comparison to aragonite. (A) Missing-atoms model of mAra showing incomplete Ca polyhedra. The coordination numbers are nine for Ca1 and Ca4 (blue polyhedra), eight for Ca3 and Ca6 (red polyhedra), seven for Ca2 (green polyhedra), and six for Ca5 (green polyhedra). (B) All-atoms mAra has ninefold coordinated Ca (blue polyhedra). (C) Standard aragonite. Black spheres mark C atoms.

fig. S4) shows substantial diffuse scattering, which renders the unit-cell determination of mAra difficult.

EDT measurements reveal that mAra has a monoclinic unit cell with parameters $b = 5.7(1) \text{ \AA}$, $c = 9.2(1) \text{ \AA}$, and $\beta = 120.2(5)^\circ$. The third cell parameter, a , runs parallel to the diffuse scattering direction and depends on the local modulation (order) of the crystal. For commensurate (periodic) modulations, the value of a is a multiple of $4.8(1) \text{ \AA}$, that is, half of the $[110]$ aragonite cell vector. For modulation-1, a is thus equivalent to $4.8(1) \text{ \AA}$, resulting in a pseudo-hexagonal monoclinic cell that may be directly converted into the orthorhombic cell of standard aragonite (section S1). Although any modulation number can be envisioned, the three-dimensional EDT reconstructions (Fig. 3) and two-dimensional SAED patterns (Fig. 2) taken from the best-ordered domains reveal a recurrent modulation-6 [$a = 28.6(7) \text{ \AA}$] (fig. S5). Therefore, we propose the following cell parameters for mAra: $a = 28.6(7) \text{ \AA}$, $b = 5.7(1) \text{ \AA}$, $c = 9.2(1) \text{ \AA}$, $\beta = 120.2(5)^\circ$, and space group $P2_1/c$ (Fig. 3).

The strong diffuse scattering renders the ab initio structure determination of mAra challenging even for the best-ordered EDT dataset (Materials and Methods). The atomic positions of the average modulation-1 structure, which accounts for the strong reflections only (satellites are neglected), fit those of standard aragonite. The ab initio structure solution for modulation-6, which contains six aragonite-like Ca polyhedra layers (Fig. 4), results instead in few missing O

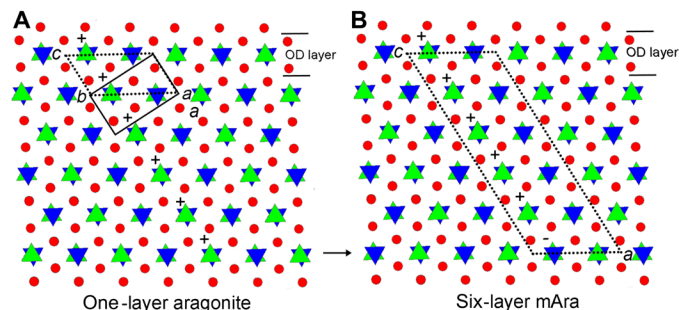


Fig. 5. Aragonite and mAra are polytypes, and their structures can be built by OD layers. $\{110\}$ slab is the basic structure unit (OD layer) of aragonite. Red spheres mark Ca atoms, and blue and green triangles correspond to CO_3 groups that differ in relative height along the aragonite (001) projection. Direction of the layer shift is marked by + and - with respect to the basic OD unit. (A) Ordinary aragonite (marked by black lines) is a one-layer polytype, in which the OD layer shift is one way (+++). Dotted lines and italicized indices mark the unit cell size and the parameters of the monoclinic modulation-1 structure, respectively. (B) The ordered modulation-6 mAra structure (marked by dotted lines) can be built by a six-layer sequence (+++---), in which there is an orientation change (marked by a black arrow) in the building OD layers.

and C atoms. This implies that not all Ca have nine O neighbors; the structure solution suggests six- to ninefold coordinated Ca, and some CO_3 groups are missing. It is possible that missing CO_3 groups are replaced by hydroxyls, similar to the reversible $\text{CO}_3^{2-} \rightleftharpoons 2\text{OH}^-$ substitution observed in hydromagnesite (30) and apatite (31). The strong diffuse scattering suggests that such (partial) substitution occurs in a rather random fashion, which cannot be quantified using diffraction data. Structure refinement was therefore performed including all expected O and C positions for aragonite at full occupancy, resulting in distorted Ca polyhedra (Fig. 4). In particular, one of the six layers is significantly expanded, with a remarkably long Ca-O distance of about 3 \AA (table S5). This supports the conclusion that not all Ca atoms in mAra are ninefold coordinated and that hydroxyl groups partially substitute CO_3 groups in a more or less ordered way.

It is intriguing that the chemical analysis of some mAra grains indicates a Mg content of up to 10 atomic % (at %) (Fig. 1D). Even the crystal showing the best-ordered EDT dataset contains ~ 2 at % Mg (fig. S4). Mg commonly occurs in six- and eightfold coordination, but ninefold coordinated Mg is unknown. Hydromagnesite and magnesite have six-coordinated Mg. In contrast, Ca has nine O neighbors in ordinary aragonite; thus, Mg cannot substitute for Ca. However, mAra has a candidate structure that can accommodate Mg in its low-coordination (lower than nine) cation sites (Fig. 4).

TEM chemical analysis is inappropriate for measuring the hydroxyl content of individual nanocrystals. Fourier transform infrared (FTIR) spectroscopy allows us to perform OH^- measurements, but the spectra collected from bulk sample on the surface of the aragonite flowstone indicate no or only a negligible amount (<0.1 at %) of hydroxyls. However, mAra is presumably a minor phase in this sample batch, and the spectra are dominated by ordinary aragonite. Therefore, the FTIR result does not preclude that mAra crystals contain carbonate-replacing hydroxyls.

According to the classical definition of polymorphism, different polymorphs must have the same chemical composition and differ only in their crystal structure. However, chemical variations, that is, deviations from the ideal formula, are common in minerals. From a mineralogical point of view, the content of Mg (and possibly of OH^-)

in mAra is not significant, so its chemical formula is close to the ideal CaCO_3 . In addition, it is possible that some mAra crystals have a pure CaCO_3 composition. Such a variable chemical formula is consistent with the precursor nature of mAra.

Aragonite polytypism and order-disorder structures

The order-disorder (OD) approach [(32) and references therein] is a powerful tool for describing and understanding the mAra structure. Makovicky (33) already used this approach for the interpretation of {110} aragonite twins. According to (33), the aragonite structure can be described on the basis of units consisting of OD layers with $b = 9.39 \text{ \AA}$, $c = 5.74 \text{ \AA}$, and a perpendicular thickness (a) of 4.21 \AA (Fig. 5). This basic unit matches the cell we propose for the monoclinic setting of modulation-1 mAra [$a = 4.8(1) \text{ \AA}$, $b = 5.7(1) \text{ \AA}$, $c = 9.2(1) \text{ \AA}$, and $\beta = 120.2(5)^\circ$]. In this setting, stacked OD layers are shifted by $1/4 c$ with respect to each other. Depending on the direction of the shift (+ or -), various polytypic sequences are obtained. For ordinary aragonite, the shift is one way (e.g., +++; Fig. 5A), whereas for twinned aragonite there is a sudden change in the shift (e.g., +++---). Following the description of Makovicky (33), the

ordered modulation-6 mAra structure can be interpreted as a six-layer polytype, in which there is an orientation change (an alternate switch; e.g., +++++-) in the building OD layers (Fig. 5B). Besides the ordered mAra structures, infinite disordered mAra sequences with randomly oriented OD layers can be envisioned, giving rise to the characteristic diffuse scattering experimentally observed along the {110} aragonite direction.

Makovicky (33) suggests that the incorporation of different-size cations might influence the probability of the orientation change of the aragonite OD layer. Similarly, CO_3 replacing OH^- may also induce a similar stacking variation. During crystal growth, Mg and OH presumably leave the system, but the ubiquitously observed diffuse scattering might be indicative for their previous occurrence.

DISCUSSION

Mechanism of aragonite formation in Mg-rich environments

Our findings reveal that mAra is the precursor phase of aragonite and the fourth CaCO_3 polymorph at near-surface conditions on Earth. Aragonite formation at ambient conditions has previously been attributed to the crystallization of an amorphous and poorly crystalline precursor (19–23). This phase, termed pAra, has not been identified in our samples, although the low temperature [$1.0(4)^\circ\text{C}$] of the studied cave likely promotes the formation and preservation of the poorly crystalline precursor phases, as shown by recent observations of samples from a cave in Hungary (34). The nanosize of crystals and diffuse scattering commonly result in an amorphous-like x-ray diffraction pattern, which can possibly be associated with ACC. In addition, the characteristic FTIR spectra of nanocrystals and disordered structures differ from those of well-crystallized phases and may give rise to ACC-similar FTIR features. For a proper structural characterization and avoiding possible misinterpretation of precursor phases, we therefore point out the necessity of single-nanocrystal analysis, which can be performed using TEM and electron diffraction.

We propose a new mechanism of aragonite formation with mAra as the first Ca-rich carbonate phase to precipitate from water with a $\text{Mg}^{2+}/\text{Ca}^{2+}$ ratio > 1.5 (Fig. 6). We suggest that this precursor forms by incorporating Mg atoms into its low-coordination cation sites and hydroxyl groups. During crystal growth, the mAra structure becomes unstable and releases Mg and hydroxyl groups to the ambient solution, thereby transforming into the closely related and more stable form of conventional orthorhombic aragonite (Fig. 5). A similar reconstructive process, accompanied by an increase in particle size, has recently been observed for the vaterite-to-calcite transformation (35).

mAra coexists with hydromagnesite and magnesite in the drip water and the flowstone samples, respectively. The transformation of hydromagnesite to magnesite via release of water has previously been proposed (36). Primary precipitation of magnesite, however, cannot be excluded. In either way, the drip water mostly yields Mg carbonates, whereas the flowstone surface layer is Ca-carbonate dominated. This difference is presumably related to the spatial variability of the drip water's chemical composition. Nevertheless, for both samples, the first Ca-containing phase is mAra that precedes the formation of aragonite.

Characteristic mAra features from biogenic and synthetic material

The characteristic mAra diffraction features are diffuse scattering and satellite reflections along aragonite {110} (Fig. 2B). Identical features

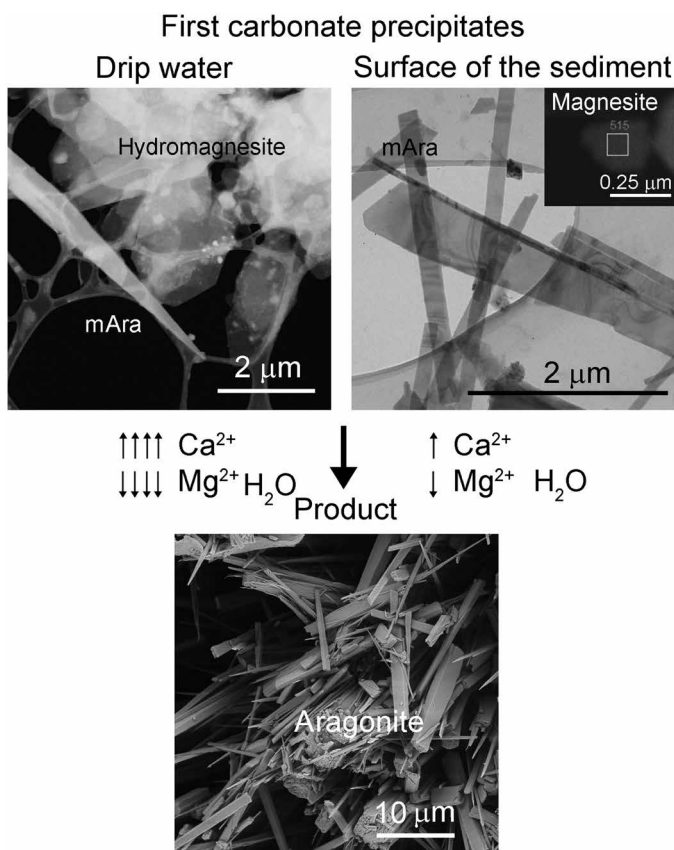


Fig. 6. Proposed mechanism for metastable aragonite formation from drip water containing a $\text{Mg}^{2+}/\text{Ca}^{2+}$ ratio > 1.5 . Initially precipitated mAra forms by incorporating Mg atoms and hydroxyl groups, which result in a disordered monoclinic structure. mAra is associated with abundant hydromagnesite in the 20-hour collected drip water and some magnesite in the flowstone samples. Abundant hydromagnesite formation is presumably related to the chemical variability of the drip water. Aragonite forms as a result of crystallographic ordering and Mg leaching from mAra. During its formation, depending on the composition of the primary phases, the Ca concentration increases, whereas Mg and water contents decrease.

have been reported from lacustrine stromatolites [figure 3C of (15)] and synthetic aragonite [figure 2D of (37)]. The streaking of reflections, observed for an aragonite crystal, which was formed by the cyanobacteria *Synechocystis* sp. PCC6803 after 75 days of cultivation in $Mg^{2+}/Ca^{2+} = 2$ environment [figure 9D of (38)], is also consistent with mAra. {110} twinning is commonly reported from mollusk shells (39), and Rodriguez-Navarro *et al.* reported polysynthetic {110} twins and streaking of reflections from the shell of the gastropod *Conus marmoreus* [figure 3B of (40)], whose characteristic features resemble those of mAra. Thus, it is plausible to assume that {110} twins are actually arising as a result of transformation of mAra to aragonite, that is, they are indicative for the precursor mAra. Therefore, we imply that mAra occurs in synthetic material as well as in a wide range of marine and lacustrine environments and plays an important role in metastable aragonite formation.

MATERIALS AND METHODS

Sample collection site and sampling

Carbonate precipitates were sampled in August 2017 from Obstanser Eishöhle, which is located 3 km south of Kartitsch (46.6875°N, 12.4932°E), close to the Austrian-Italian border. Aragonite was actively precipitating in this cave from drip water containing $Mg^{2+}/Ca^{2+} > 1.5$ and occurred as snow-white flowstones and stalactites in a close vicinity to hydromagnesite and calcite (26). We collected precipitates both (i) from the stalactite drip water and (ii) from the surface of aragonite flowstone covering the cave wall (fig. S1). (i) To sample drip water precipitates, we drilled the bottom of a TEM grid box so that drip water could flow through the hole during carbonate precipitation. We inserted lacey-C-coated Cu TEM grids (Agar Scientific) into the grid box and placed it under the drip water for 20 hours. (ii) To collect precipitates from the surface of the aragonite flowstone, we placed a TEM grid into self-locking tweezers and gently touched the aragonite surface three times. This sample collection procedure permitted the study of the freshly deposited and loosely bound carbonates. Taking the studied flowstone's aragonite growth rate of 34 $\mu\text{m}/\text{year}$ (26) into account and using a maximum thickness estimate of ~10 to 20 μm (crystals shown in the TEM figures are from the thin part of the sample) for the material on the TEM sample holder, the sampled carbonate of the flowstone surface likely corresponded to less than 1 year of precipitation. We analyzed the drip water and flowstone precipitates using TEM.

TEM measurement, data collection, structure determination, and refinement

Bright-field TEM (BFTEM) images and two-dimensional SAED patterns were taken with a Philips CM20 electron microscope operating at 200 keV. BFTEM images and SAED patterns were recorded on imaging plates. Dark-field scanning TEM images and EDT data were taken with a Zeiss Libra 120 electron microscope operating at 120 kV and equipped with a LaB₆ thermionic gun, a Nanomegas Spinning-star device for beam precession, and an ASI Medipix single-electron detector for electron diffraction recording. EDT data were acquired at steps of 1° with a beam precession semi-angle of 1° following the protocol described in (41). Data analysis, including three-dimensional diffraction volume reconstruction, cell parameter determination, and reflection intensity integration, were performed using ADT3D software (41) and in-home developed Matlab routines. Details of the EDT measurement were reported in tables S1 and S2. Energy-dispersive x-ray

microanalysis was performed using a NORAN Voyager system and a Bruker EDX XFlash6T-60 detector attached to the Philips and ZEISS electron microscopes, respectively. For the matrix-based unit-cell transformation, the Crystal Cracker software (http://multianvil.usu.edu/Crystal_Cracker/CrystalCracker.html) was used.

Ab initio structure determination, assuming kinematical approximation with $I_{hkl} \sim F_{hkl}^2$, was performed by direct methods implemented in the SIR2014 software (42). Least-squares structure refinement was performed by SHELXL (43). Data were reported in tables S1 to S5 and data files S1 to S5.

Ab initio structure determination of hydromagnesite

Three datasets from three platy hydromagnesite crystals were collected using EDT. Their measurements were consistent with the following monoclinic cell parameters: $a = 9.9(1) \text{ \AA}$, $b = 8.9(1) \text{ \AA}$, $c = 8.5(1) \text{ \AA}$, $\beta = 114.4(5)^\circ$. Crystallographic extinctions suggested space group $P2_1/c$, which was in good agreement with published data (30) for this mineral ($P2_1/c$, $a = 10.105 \text{ \AA}$, $b = 8.954 \text{ \AA}$, $c = 8.378 \text{ \AA}$, $\beta = 114.44^\circ$). The ab initio structure determination of a selected crystal (fig. S2) and refinement of its EDT data resulted in reasonable refinement parameters (table S3) and literature data matching Mg, C, and O atomic positions (table S4). The cif structure data and measured hkl file were reported in data files S1 and S2, respectively.

Ab initio structure determination and structure refinement of mAra

The ab initio structure determination resulted in a model in which five atoms (three C and two O) were missing compared to the expected stoichiometry for aragonite. We refined this model using SHELXL and obtained an overall agreement R value of 0.4908 (table S2). Using restraints (SADI on C–O distances and FLAT for CO₃ triangles), we placed the missing C and O atoms into the model and refined it. The all-atoms model refinement resulted in an overall R value of 0.3861, which was lower than that of the missing-atoms model. For both models, the thermal factors were positive and scattered in a reasonable range (table S4).

The missing-atoms model contained Ca in six- to ninefold coordination, whereas the coordination number of all Ca atoms was nine in the all-atoms mAra model (Fig. 4). The Ca–O bond distances for this refined model were shown in table S5. The cif structure data of missing and all atoms and the measured hkl file were reported in data files S3 to S5.

SUPPLEMENTARY MATERIALS

Supplementary material for this article is available at <http://advances.sciencemag.org/cgi/content/full/4/12/eaa6178/DC1>

Section S1. Crystallographic relationship between mAra and aragonite

Fig. S1. Sample collection sites.

Fig. S2. The EDT measured hydromagnesite grain from the drip water sample.

Fig. S3. Magnesite coexisting with mAra in the sample collected from the surface of the aragonite flowstone.

Fig. S4. Chemical analysis of the mAra crystal measured by EDT (Fig. 3) indicates ~2 at % Mg.

Fig. S5. Satellite reflections of the SAED patterns (2 and 3 of Fig. 2) can be indexed with the mAra (monoclinic-6) unit cell.

Table S1. Summary of EDT data for hydromagnesite and mAra.

Table S2. Summary of structure refinements of hydromagnesite and mAra.

Table S3. EDT-measured and SHELXL-refined hydromagnesite atomic coordinates (x_1, y_1, z_1) versus literature data (x_2, y_2, z_2) of (30).

Table S4. Atomic coordinates and equivalent isotropic displacement parameters (U_{iso} in \AA^2) for the ab initio determined, missing-atoms (x_1, y_1, z_1, U_{iso1}) and all-atoms refined (x_1, y_1, z_1, U_{iso2}) mAra structures.

Table S5. Ca–O bond distances (in angstrom units) for the all-atoms refined mAra structure.

Data file S1. (Hydromagnesite.cif) cif file of the measured hydromagnesite.
 Data file S2. (Hydromagnesite.hkl) hkl file of the measured hydromagnesite.
 Data file S3. (Missing-atoms mAra.cif) cif file of the missing-atoms mAra.
 Data file S4. (All-atoms mAra.cif) cif file of the all-atoms mAra.
 Data file S5. (mAra.hkl) hkl file of the measured mAra.

REFERENCES AND NOTES

- D. Gebauer, A. Völkel, H. Cölfen, Stable prenucleation calcium carbonate clusters. *Science* **322**, 1819–1822 (2008).
- E. M. Pouget, P. H. H. Bomans, J. A. C. M. Goos, P. M. Frederik, G. de With, N. A. J. M. Sommerdijk, The initial stages of template-controlled CaCO₃ formation revealed by cryo-TEM. *Science* **323**, 1455–1458 (2009).
- E. Mugnaioli, I. Andrusenko, T. Schüler, N. Loges, R. E. Dinnebier, M. Panthöfer, W. Tremel, U. Kolb, Ab initio structure determination of vaterite by automated electron diffraction. *Angew. Chem. Int. Ed. Engl.* **51**, 7041–7045 (2012).
- J. W. Morse, F. T. Mackenzie, *Geochemistry of Sedimentary Carbonates* (Elsevier, 1990).
- N. P. James, B. Jones, *Origin of Carbonate Sedimentary Rocks* (Wiley, 2016).
- V. De Choudens-Sánchez, L. A. González, Calcite and aragonite precipitation under controlled instantaneous supersaturation: Elucidating the role of CaCO₃ saturation state and Mg/Ca ratio on calcium carbonate polymorphism. *J. Sediment. Res.* **79**, 363–376 (2009).
- S. Riechelmann, A. Schröder-Ritzrau, J. A. Wassenburg, J. Schreuer, D. K. Richter, D. F. C. Riechelmann, M. Terente, S. Constantin, A. Mangini, A. Immenhauser, Physicochemical characteristics of drip waters: Influence on mineralogy and crystal morphology of recent cave carbonate precipitates. *Geochim. Cosmochim. Acta* **145**, 13–29 (2014).
- W. Sun, S. Jayaraman, W. Chen, K. A. Persson, G. Ceder, Nucleation of metastable aragonite CaCO₃ in seawater. *Proc. Natl. Acad. Sci. U.S.A.* **112**, 3199–3204 (2015).
- S. W. Wise Jr., Microarchitecture and deposition of gastropod nacre. *Science* **167**, 1486–1488 (1970).
- P. U. P. A. Gilbert, R. A. Metzler, D. Zhou, A. Scholl, A. Doran, A. Young, M. Kunz, N. Tamura, S. N. Coppersmith, Gradual ordering in red abalone nacre. *J. Am. Chem. Soc.* **130**, 17519–17527 (2008).
- G. Falini, S. Albeck, S. Weiner, L. Addadi, Control of aragonite or calcite polymorphism by mollusk shell macromolecules. *Science* **271**, 67–69 (1996).
- D. Allemand, É. Tambutté, D. Zoccola, S. Tambutté, Coral calcification, cells to reefs. *Coral Reefs: An Ecosystem in Transition*, Z. Dubinsky, N. Stambler, Eds. (Springer, 2011).
- A. M. Smith, M. A. Riedi, D. J. Winter, Temperate reefs in a changing ocean: Skeletal carbonate mineralogy of serpulids. *Mar. Biol.* **160**, 2281–2294 (2013).
- G. Falini, S. Fermani, S. Vanzo, M. Miletic, G. Zaffino, Influence on the formation of aragonite or vaterite by otolith macromolecules. *Eur. J. Inorg. Chem.* **2005**, 162–167 (2005).
- K. Benzerara, A. Meibom, Q. Gautieri, J. Kazmierczak, J. Stolarski, N. Menguyi, G. Brown, *Nanotextures of Aragonite in Stromatolites from the Quasi-Marine Satonda Crater Lake, Indonesia* (Geological Society, 2010).
- H. H. Teng, P. M. Dove, C. A. Orme, J. J. De Yoreo, Thermodynamics of calcite growth: Baseline for understanding biomineral formation. *Science* **282**, 724–727 (1998).
- G. F. Camoin, P. Gautret, Microbialites and microbial communities: Biological diversity, biogeochemical functioning, diagenetic processes, tracers of environmental changes. *Sediment. Geol.* **185**, 127–130 (2006).
- S. Weiner, I. Sagi, L. Addadi, Choosing the crystallization path less traveled. *Science* **309**, 1027–1028 (2005).
- T. Mass, A. J. Giuffrè, C.-Y. Sun, C. A. Stiffler, M. J. Frazier, M. Neder, N. Tamura, C. V. Stan, M. A. Marcus, P. U. P. A. Gilbert, Amorphous calcium carbonate particles form coral skeletons. *Proc. Natl. Acad. Sci. U.S.A.* **114**, E7670–E7678 (2017).
- R. T. DeVol, C.-Y. Sun, M. A. Marcus, S. N. Coppersmith, S. C. B. Myneni, P. U. P. A. Gilbert, Nanoscale transforming mineral phases in fresh nacre. *J. Am. Chem. Soc.* **137**, 13325–13333 (2015).
- K. K. Sand, J. D. Rodríguez-Blanco, E. Makovicky, L. G. Benning, S. L. S. Stipp, Crystallization of CaCO₃ in water–alcohol mixtures: Spherulitic growth, polymorph stabilization and morphology change. *Cryst. Growth Des.* **12**, 842–853 (2012).
- M. Farhadi-Khouzani, D. M. Chevrier, P. Zhang, N. Hedin, D. Gebauer, Water as the key to proto-aragonite amorphous CaCO₃. *Angew. Chem. Int. Ed. Engl.* **55**, 8117–8120 (2016).
- J. M. Walker, B. Marzec, F. Nudelman, Solid-state transformation of amorphous Calcium carbonate to aragonite captured by cryoTEM. *Angew. Chem. Int. Ed. Engl.* **56**, 11740–11743 (2017).
- Z. Zhang, Y. Xie, X. Xu, H. Pan, R. Tang, Transformation of amorphous calcium carbonate into aragonite. *J. Cryst. Growth* **343**, 62–67 (2012).
- A. V. Radha, T. Z. Forbes, C. E. Killian, P. U. P. A. Gilbert, A. Navrotsky, Transformation and crystallization energetics of synthetic and biogenic amorphous calcium carbonate. *Proc. Natl. Acad. Sci. U.S.A.* **107**, 16438–16443 (2010).
- C. Spötl, J. Fohlmeister, H. Cheng, R. Boch, Modern aragonite formation at near-freezing conditions in an alpine cave, Carnic Alps, Austria. *Chem. Geol.* **435**, 60–70 (2016).
- U. Kolb, T. Gorelik, C. Kübel, M. T. Otten, D. Hebert, Towards automated diffraction tomography: Part I—Data acquisition. *Ultramicroscopy* **107**, 507–513 (2007).
- U. Kolb, E. Mugnaioli, T. E. Gorelik, Automated electron diffraction tomography—A new tool for nano crystal structure analysis. *Cryst. Res. Technol.* **46**, 542–554 (2011).
- E. Mugnaioli, M. Gemmi, Single-crystal analysis of nanodomains by electron diffraction tomography: Mineralogy at the order-disorder borderline. *Z. Kristallogr.* **233**, 163–178 (2018).
- M. Akao, S. Iwai, The hydrogen bonding of hydromagnesite. *Acta Crystallogr. Sect. B Struct. Sci.* **33**, 1273–1275 (1977).
- M. E. Fleet, X. Liu, Coupled substitution of type A and B carbonate in sodium-bearing apatite. *Biomaterials* **28**, 916–926 (2007).
- S. Đurović, Fundamentals of the OD theory, in *Modular Aspects of Minerals, EMU Notes in Mineralogy, Vol. 1* (Eötvös University Press, 1997), pp. 3–28.
- E. Makovicky, Twinning of aragonite—The OD approach. *Mineral. Petrol.* **106**, 19–24 (2012).
- A. Demény, P. Németh, Gy. Czuppon, Sz. Leél-Össy, M. Szabó, K. Judik, T. Németh, J. Stieber, Formation of amorphous calcium carbonate in caves and its implications for speleothem research. *Sci. Rep.* **6**, 39602 (2016).
- M. Dietzsch, I. Andrusenko, R. Branscheid, F. Emmerling, U. Kolb, W. Tremel, Snapshots of calcium carbonate formation—A step by step analysis. *Z. Kristallogr.* **232**, 255–265 (2017).
- M. Hänchen, V. Prigiobbe, R. Baciocchi, M. Mazzotti, Precipitation in the Mg-carbonate system—Effects of temperature and CO₂ pressure. *Chem. Eng. Sci.* **63**, 1012–1028 (2008).
- S.-H. Yu, H. Li, Q.-Z. Yao, S.-Q. Fuc, G.-T. Zhou, Hierarchically nanostructured shuttle-like aragonite mesocrystals: Preparation, characterization, growth mechanism, and removal ability to La(III). *J. Environ. Chem. Eng.* **5**, 893–905 (2017).
- Z. Han, R. Meng, H. Yan, H. Zhao, M. Han, Y. Zhao, B. Sun, Y. Sun, J. Wang, D. Zuang, W. Li, L. Lu, Calcium carbonate precipitation by *Synechocystis* sp. PCC6803 at different Mg/Ca molar ratios under the laboratory condition. *Carbonates Evaporites* **32**(4), 561–575 (2017).
- T. Kogure, M. Suzuki, H. Kim, H. Mukai, A. G. Checa, T. Sasaki, H. Nagasawa, Twin density of aragonite in molluscan shells characterized using X-ray diffraction and transmission electron microscopy. *J. Cryst. Growth* **307**, 39–46 (2014).
- A. B. Rodríguez-Navarro, A. Checa, M. G. Willinger, R. Bolmaro, J. Bonarski, Crystallographic relationships in the crossed lamellar microstructure of the shell of the gastropod *Conus marmoreus*. *Acta Biomater.* **8**, 830–835 (2012).
- E. Mugnaioli, T. Gorelik, U. Kolb, “Ab initio” structure solution from electron diffraction data obtained by a combination of automated diffraction tomography and precession technique. *Ultramicroscopy* **109**, 758–765 (2009).
- M. C. Burla, R. Caliandro, B. Carrozzini, G. L. Cascarano, C. Cuocci, C. Giacovazzo, M. Mallamo, A. Mazzone, G. Polidori, Crystal structure determination and refinement via *SIR2014*. *J. Appl. Cryst.* **48**, 306–309 (2015).
- G. M. Sheldrick, A short history of SHELX. *Acta Crystallogr. A* **68**, 112–122 (2008).

Acknowledgments: We are grateful for access to the microscope facilities in the Thin Film Physics Department—TEM & HREM Laboratory at Institute of Technical Physics and Materials Science (Budapest) and in the Center for Nanotechnology Innovation@NEST at IIT (Pisa). We thank G. Ferraris for valuable discussion on polymorphism and polytypism and appreciate the insightful comments of the journal reviewers. **Funding:** We acknowledge financial support by the Hungarian National Research, Development and Innovation Office project NKFIH_123871, the bilateral short-term mobility program provided by the Hungarian and Austrian Academies of Sciences, and the University of Innsbruck. P.N. and G.C. acknowledge the financial support of the János Bolyai Research Scholarship. E.M. and M.G. acknowledge the Regione Toscana for funding the purchase of the Timepix detector through the FELIX project (Por CREO FESR 2014-2020 action). **Author contributions:** P.N., G.C., and C.S. initiated the project and collected the samples. P.N. performed the BFTEM and SAED investigations, and took the lead on manuscript writing. E.M. measured the samples with EDT and determined the crystal structures. E.M., M.G., A.D., and C.S. substantially contributed to manuscript writing. All authors approved the manuscript. **Competing interests:** The authors declare that they have no competing interests. **Data and materials availability:** All data needed to evaluate the conclusions in the paper are present in the paper and/or the Supplementary Materials. Additional data related to this paper may be requested from the authors.

Submitted 28 June 2018
 Accepted 15 November 2018
 Published 12 December 2018
 10.1126/sciadv.aau6178

Citation: P. Németh, E. Mugnaioli, M. Gemmi, G. Czuppon, A. Demény, C. Spötl, A nanocrystalline monoclinic CaCO₃ precursor of metastable aragonite. *Sci. Adv.* **4**, eaau6178 (2018).

A nanocrystalline monoclinic CaCO_3 precursor of metastable aragonite

Péter Németh, Enrico Mugnaioli, Mauro Gemmi, György Czuppon, Attila Demény and Christoph Spötl

Sci Adv 4 (12), eaau6178.

DOI: 10.1126/sciadv.aau6178

ARTICLE TOOLS

<http://advances.sciencemag.org/content/4/12/eaau6178>

SUPPLEMENTARY MATERIALS

<http://advances.sciencemag.org/content/suppl/2018/12/10/4.12.eaau6178.DC1>

REFERENCES

This article cites 38 articles, 10 of which you can access for free
<http://advances.sciencemag.org/content/4/12/eaau6178#BIBL>

PERMISSIONS

<http://www.sciencemag.org/help/reprints-and-permissions>

Use of this article is subject to the [Terms of Service](#)